IEEE Photonics Journal
An IEEE Photonics Society Publication

Cascaded Dual-Soliton Pulse Stokes for Broadband Coherent Anti-Stokes Raman Spectroscopy

Volume 8, Number 6, December 2016

Kun Chen
Tao Wu
Tian Zhou
Haoyun Wei
Yan Li

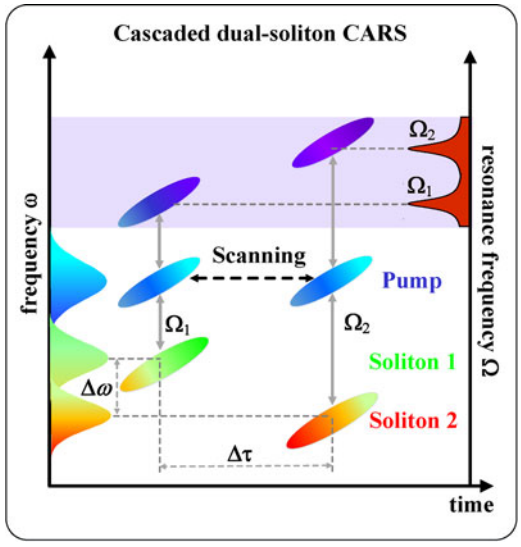

DOI: 10.1109/JPHOT.2016.2629084
1943-0655 © 2016 IEEE

Cascaded Dual-Soliton Pulse Stokes for Broadband Coherent Anti-Stokes Raman Spectroscopy

Kun Chen, Tao Wu, Tian Zhou, Haoyun Wei, and Yan Li

Key Lab of Precision Measurement Technology and Instrument, Department of Precision Instrument, Tsinghua University, Beijing 100084, China

DOI:10.1109/JPHOT.2016.2629084

Manuscript received October 21, 2016; accepted November 12, 2016. Date of publication November 17, 2016; date of current version December 5, 2016. This work was supported in part by the State Key Laboratory of Precision Measurement Technology and Instrument of Tsinghua University and in part by the Tsinghua University Initiative Scientific Research Program, and by the National Scientific Instrument and Equipment Development Projects of China (2013yq7067502). Corresponding author: H. Wei.

Abstract: We report a spectrally and temporally cascaded dual-soliton Stokes excitation source for broadband coherent anti-Stokes Raman spectroscopy (CARS) based on a single Yb-doped fiber laser. The strong birefringence of a polarization-maintaining photonic crystal fiber has the potential to simultaneously generate two solitons along different eigenpolarization axes, allowing for an extra degree of freedom in tuning the properties of the supercontinuum. With well-separated spectral regions of this dual-soliton, the CARS spectral coverage can be greatly extended. Taking advantage of the dispersion characteristic of the two orthogonal polarized modes and applying identical linear frequency chirp on both soliton Stokes pulses further allows that spectral CARS information can be encoded and acquired in time. The chirped pump pulse, in conjunction with dual-soliton Stokes pulses, can potentially yield gapless coverage of Raman transitions from 800 to 1800 cm^{-1} with a spectral resolution of 15 cm^{-1}. Broadband spectral coverage capability is theoretically verified with simulations and then experimentally demonstrated by CARS spectroscopy with varied polymer materials. We also demonstrate hyperspectral Raman microscopy with molecular contrast of lipid droplets. An all-fiber-based broadband excitation source may greatly simplify CARS implementation and extend the qualitative and even quantitative chemical analysis of CARS microspectroscopy.

Index Terms: Ultrafast nonlinear processes, Raman spectroscopy, non-linear microscopy.

1. Introduction

Over the past decade, coherent anti-Stokes Raman scattering microscopy has been used increasingly as a noninvasive microscopic tool in biophysics, biology, and material sciences, offering 3-D sectioning capability and chemical specificity without the need of staining and fluorescence tagging [1]–[3]. CARS originates from a four-wave mixing process between the pump at frequency ω_p and the Stokes at frequency ω_s, and the intensity of the anti-Stokes at $\omega_{as} = 2\omega_p$-ω_s is measured. Therefore, the current gold-standard CARS system generally requires two sequences of pulses from synchronized and feedback controlled picosecond (ps) solid-state oscillators or synchronously pumped ps optical parametric oscillators (OPOs) to achieve a satisfactory spectral resolution and video-rate imaging [4]. Nevertheless, chemical specificity in the original implementation of CARS microscopy remains limited because a CARS image reflects just a single vibrational mode [4]–[6]. It is, therefore, difficult to specifically detect molecules with overlapping Raman bands, especially

in the crowded fingerprint region. Even the combination of a spectrally narrow pump pulse and a spectrally broad Stokes pulse with a spectrometer can cover several hundred wavenumbers and allow one to detect different molecules simultaneously, this technique still suffers from limitations in the Stokes pulse breadth [7]. Tunable excitation source offers a versatile way to alleviate this problem in practical application. For example, the state-of-the-art synchronously pumped OPO can cover the entire chemically vibrational frequency range of 100–3700 cm^{-1} [8], [9], because its signal and idler beams can be both continuously tunable. Although many demonstrations have been reported so far in the fields of life sciences [10], [11], material sciences [12], [13], and chemistry [14], [15], this solid OPOs still suffers from the tuning speed and complexity of the light sources, such as their active feedback temperature-controlled configuration, their large footprint (> 2 m^2), and their expensive price.

In contrast to the free space lasers, all-fiber based excitation source could be used in less favorable environments while being attractively compact and low-cost. Recently, Er- and Yb-doped fiber lasers combined with highly nonlinear fiber or PCF have been put to use in a new type of all-fiber-optic coherent Raman microscopy [16]. Meanwhile, transform-limited (TL) output soliton pulses can also be achieved by taking advantage of the nonlinearities of a PCF in the anomalous dispersion regime due to the balance between anomalous dispersion and the Kerr nonlinearity [17]. It opens the door to spectroscopic applications and hyperspectral imaging, offering a feasible route at solving the precompensation problem [18]. However, one can only cover a piece of specific Raman spectrum in one measurement because of the narrow spectral width of the soliton pulses. It significantly limits the characterization of chemical information from multiple vibration peaks of different molecules. Even though the wavelength tunability of the soliton based on self-frequency shift (SSFS) can be achieved [19]–[22], it is time consuming and is difficult to attain stable soliton pulses during the tuning process which further disrupt real-time and quantitative hyperspectral imaging.

In this paper, we present a broadband CARS system that efficiently stimulates Raman transitions throughout the entire fingerprint region, using spectrally and temporally cascaded dual-soliton Stokes pulses, and exploits the linear chirp to improve the spectral resolution. This well-defined dual-soliton stem from a strongly birefringent and highly nonlinear PM-PCF simultaneously along and both serve as Stokes pulses. The chirped pump pulse in conjunction with dual-soliton Stokes pulses can potentially yield gapless coverage of Raman transitions from 800 to 1800 cm^{-1} with a spectral resolution of 15 cm^{-1}, by scanning the time delay between the two beams. We theoretically and experimentally demonstrate the broadband CARS spectroscopy with varied polymer materials. For microscopy purpose, we also demonstrate hyperspectral Raman imaging with molecular contrast of lipid droplets. This all-fiber-based broadband excitation source can greatly simplify CARS implementation and broadband CARS microspectroscopy allows for excellent capability in quantitative label-free imaging of different molecules with rich chemical information from multiple characteristic vibration peaks.

2. Materials and Methods

2.1. Simulation of Dual-Soliton Generation

The basic mechanism underlying the generation of supercontinuum in a highly birefringent PCF is the fission of higher-order solitons due to high-order dispersion and nonlinear effects [23]. The interplay between the strong nonlinearity and the high birefringence has been reported previously as being the mechanism leading to dual-soliton pulses generation along different axis [24], [25]. Here, we further demonstrate that it is feasible to attain two solitons with well-separated spectral regions by carefully controlling the input polarization and the injected power in simulation using coupled vector nonlinear Schrödinger equations (VNLSE) [26]

$$\frac{\partial u}{\partial z} = i\beta u - \delta\frac{\partial u}{\partial t} + \sum_{k=2-6}\frac{i^{k+1}}{k!}\beta_k\frac{\partial^k u}{\partial t^k} + i\gamma\left(|u|^2 + \frac{2}{3}|v|^2 + \frac{i}{\omega_0}\frac{1}{u}\frac{\partial}{\partial t}\left(|u|^2 u\right)\right)u$$
$$+ i\gamma\left(1 + \frac{i}{\omega_0}\frac{\partial}{\partial t}\right)\left[u\int_0^\infty R\left(t'\right)\left|u\left(t-t'\right)\right|^2 dt'\right] + \frac{i\gamma}{3}v^2u^* \quad (1)$$

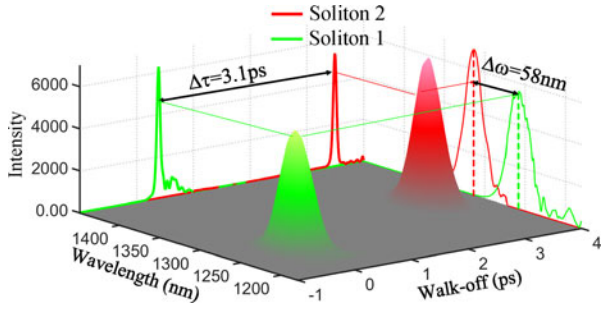

Fig. 1. Simulation of dual-soliton output of the PM-PCF when the angle between the input polarization and the fast axis is 34°. Frequency separation between soliton 1 and 2 is about $\Delta\omega = 58$ nm. Temporal walk-off is about $\Delta\tau_0 = 3.1$ ps.

$$\frac{\partial v}{\partial z} = -i\beta v + \delta\frac{\partial v}{\partial t} + \sum_{k=2-6}\frac{i^{k+1}}{k!}\beta_k\frac{\partial^k u}{\partial t^k} + i\gamma\left(|v|^2 + \frac{2}{3}|u|^2 + \frac{i}{\omega_0}\frac{1}{v}\frac{\partial}{\partial t}\left(|v|^2 v\right)\right)v$$
$$+ i\gamma\left(1 + \frac{i}{\omega_0}\frac{\partial}{\partial t}\right)\left[v\int_0^\infty R\left(t'\right)\left|v\left(t-t'\right)\right|^2 dt'\right] + \frac{i\gamma}{3}u^2 v^* \quad (2)$$

$$R\ (\mathrm{t}) = (1-f_b)\left(\tau_1^{-2}+\tau_2^{-2}\right)\tau_1\exp\left(-\frac{t}{\tau_2}\right)\sin\left(\frac{t}{\tau_1}\right) + f_b\frac{2\tau_b - t}{\tau_b^2}\exp\left(-\frac{t}{\tau_b}\right) \quad (3)$$

where u and v are the normalized envelopes of the optical pulses in the two orthogonal polarized modes. β is the wave-number difference between the two modes. $2\delta = 2\beta\lambda/2\pi c$ is the inverse group velocity difference. β_k is the k^{th}-order dispersion coefficient. f_b represents the fractional contribution of the delayed Raman response to nonlinear polarization. $\tau_1 = \Omega_R$ and Ω_R is the vibrational frequency of silica molecules. τ_2 is the damping time of vibrations. The boson peak width is $\tau_b = 96$fs. γ is the nonlinear coefficient. All of the parameters used in our simulations possibly match the experimental conditions. Specifically, a commercial PM-PCF (NKT Photonics SC-5.0–1040-PM) acts as the high birefringent fiber in practice. Therefore, $k'' = -4.2\ \mathrm{ps^2km-1}$, $k''' = 0.0681\ \mathrm{ps^3km-1}$, $\gamma = 10\,\mathrm{W^{-1}km^{-1}}$, polarization beat length = 6.3 mm, and PCF length = 193 cm.

Governed by the VNLSE, numerically simulated results in Fig. 1 qualitatively display the generated spectra and soliton pulse profiles. When the input polarization isn't parallel to the fast or slow axes, contour plots of the spectra provides an unambiguous proof that the generated spectrum is a linear combination of two continua generated separately along the two principal axes. Indeed, spectral components along one axis are not coupled to those in the other axis. This is attributable to the different dispersion characteristics of the two eigenpolarizations. It is worth noting that both frequency separation and temporal interval between dual-soliton pulses can be easily adjusted by rotating the input polarization [24]. We have demonstrated that slight difference between the dual-soliton, which is comparable to the bandwidth of the measured Raman bands can be used to achieve background-free CARS and further quantitative chemical imaging [24], [27]. Here, unlike the previous dual-soliton characteristics, we first demonstrate that the dual-soliton can have large spectral separation to facilitate broadband CARS application. As an example, Fig. 1 presents a typical dual-soliton output by carefully adjusting the input polarization angle at 34°. Soliton 2 shifts about 58 nm relative to soliton 1, towards to as long wavelength as 1350 nm. Thus, the spectrally cascaded dual-soliton can cover a broader spectrum band (~100 nm) than each one of them. Different dispersion characteristics at different wavelength and superposed on the dispersion difference along different eigenpolarizations leads to a significant temporal walk-off of dual-soliton ($\tau 0 = 3.1$ps). Enlarging the temporal separation enables high-speed imaging with a single detector in the dual-soliton scheme.

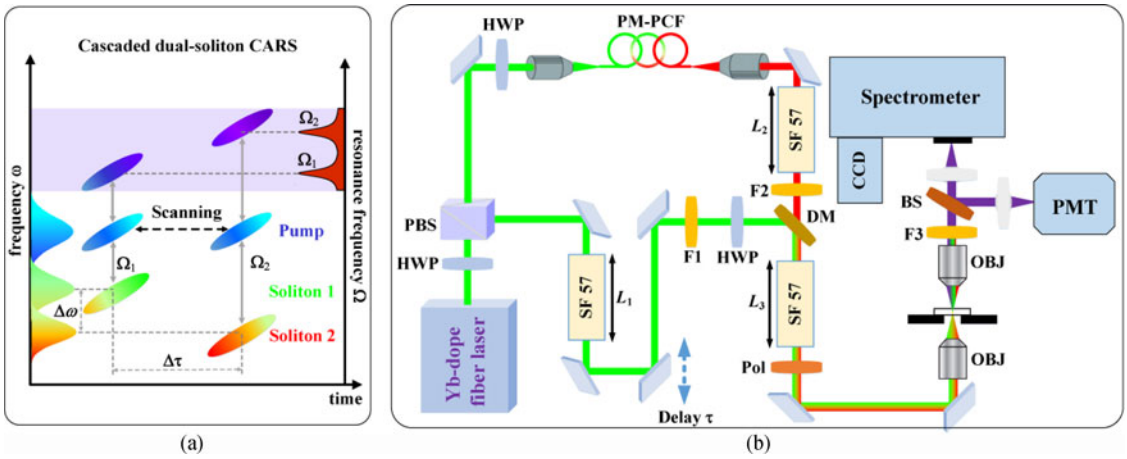

Fig. 2. (a) Time-frequency plots of the broadband dual-soliton CARS scheme; $\Delta\tau$ is the temporal walk-off of the dual-soliton pulses; $\Delta\omega$ is the frequency separation between the dual-soliton pulses. Ω_1 and Ω_2 are the Raman vibration levels. (b) Sketch of the experimental setup: HWP, half wave-plate; PBS, polarizing beam splitter; PCF, photonic crystal fiber; F1, F2, long-pass filter; F3, short-pass filter; SF57, SF-57 glass rod; DM, dichroic mirror; OBJ, objective lenses; BS, beamsplitter; PMT, photomultiplier tube; $L_1 = 30$ mm, $L_2 = 108$ mm, and $L_3 = 200$ mm.

2.2. Broadband Dual-Soliton CARS and Experimental Setup

In the CARS process, molecules are excited by two input light fields, a pump pulse and a Stokes pulse, whose frequency difference is chosen to match the frequency of Raman active transitions. If transform limited femtosecond pulses are used, the signal size increases at the expense of reduced spectral resolution. A straightforward way, known as spectral focusing method is to equally apply a linear temporal chirp on both pump and Stokes pulses to resolve the conflict [28]–[32]. The temporal walk-off dual-soliton pulses can be intrinsically applied to the spectral focusing scheme, which performs CARS spectroscopy by sequentially sweeping the interpulse delay between pump and Stokes pulses in a resonant CARS experiment, as shown in Fig. 2(a). Conceptually, the initial population of the excited vibrational state in CARS corresponds to the difference frequency generation process. For a positive delay, the frequency components of pump beam interact with that of the first soliton Stokes beam. Thus, low-frequency Raman resonance is probed. In contrast, increasing the pump pulse delay results in probing high-frequency Raman resonance. From this, it follows that the delay-scanning of pump pulse directly maps the broadband Raman shift within the spectral difference range between the pump and the two soliton pulses. Because the temporal walk-off τ_0 is larger than the chirped pulse duration, spectral CARS information can be encoded and acquired in time without aliasing.

The implementation of broadband dual-soliton CARS proceeds as presented in Fig. 2(b). A home-built Yb-doped fiber laser with an output of 2 W average power at 100 MHz repetition rate was used as the primary source. This laser output was split into the pump and the Stokes paths. SF57 glass rods with different length are added to ensure that the same amount of linear positive chirp are applied to both pump and Stokes beam. After traveling through these high-index glass rod, the pulse durations of pump and Stokes pulses are measured to be several picoseconds with an autocorrelator (APE-Berlin). A motorized delay line is inserted into the pump beam to scan the delay between the two pulse trains. These two beams are overlapped in space by a dichroic mirror and sent into a custom-made scanning microscope with a near-infrared optimized excitation objective lens (NA = 0.65, LCPLN50XIR, Olympus), and the collection objective is the same as the excitation one. The signal at anti-Stokes frequency is detected in the forward direction by means of a photomultiplier tube or an imaging spectrograph (IsoPlane160, Princeton Instruments) attached with a back-illuminated, deep depletion charge-coupled device. For imaging, the sample is raster scanned. Most of CARS measurements in this work are performed with the pump power of 50.0 mW.

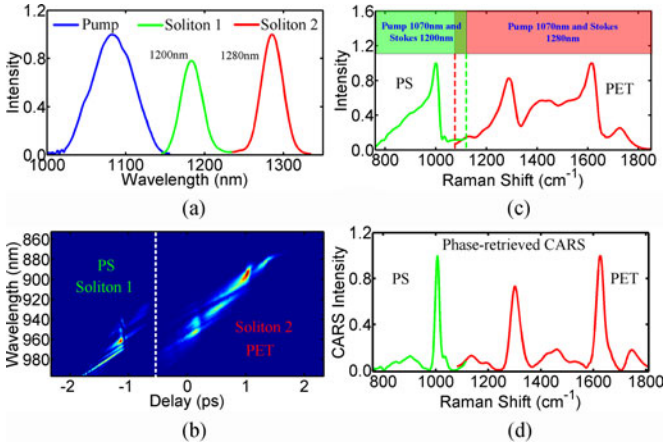

Fig. 3. (a) Spectra of pump and two soliton Stokes. (b) Measured CARS spectrograms of PS and PET as a function of pulse delay and the signal wavelength using spectrometer. For the measurement of PS, delay scanning of is from –2.3 to –0.6 ps when pump pulse interacts with soliton 1, while for PET, delay scanning is from –0.6 ∼ –2.3 ps when pump pulse interacts with soliton 1. (c) Measured raw CARS of PS beads and PET film with soliton 1 and 2, covering from 800-1800 cm^{-1}. (d) Phase-retrieved CRAS spectra using MEM method.

Standard sample with known spontaneous Raman peaks are used to calibrate the linear coefficient between the optical delay and Raman wavenumber. The nonresonant background of all the measured raw CARS spectra are removed by using the phase-retrieved method transform and the maximum entropy method (MEM) [33].

2.3. Sample Preparation

For broadband dual-soliton CARS acquisition, two kinds of polymer materials, Polystyrene (PS) beads with 20 μm diameter and polyethylene glycol terephthalate (PET) with the thickness of 200 μm were directly used. For hyperspectral imaging, the fatty acids used in this work are fish oil (Nature's Bounty, USA) and olive oil (Betis, Spainsh) and used without further purification. PS beads and oil droplets mixture are prepared in the following way: PS beads with 98% water is firstly prepared. 0.1 g of each oil is mixed with 0.1 g of Triton X-100 (Sigma-Aldrich) and stirred for 10 min, and 10 mL of water is added to the mixture, which is stirred further for 2 h. Separately prepared olive, fish oil droplets and PS beads are mixed afterward. A drop of mixture solution was pipetted inside a 120 μm thick imaging spacer (GraceTMBio-Lab SecureSealTM) glued on a glass slide (1 mm thick) in order to create a chamber, which was sealed by a second coverslip (0.13 mm thick) on top.

3. Results

We first address the broadband CARS spectra in the cascaded dual-soliton scheme. In Fig. 3(a), the pump pulse directly stems from the fiber laser with spectral width of 60 nm (center wavelength at 1070 nm). For efficient Stokes generation, about 650 mW is coupled into a 192 cm highly nonlinear PM-PCF (coupling efficiency ∼30%). Soliton 1 and 2 redshifts to about 1200 and 1280 nm, respectively, by adjusting the input power to the PCF using a half wave-plate and polarizing beam splitter combination. The power of soliton 1 and 2 are 8.0 mW and 9.5 mW, respectively. The cascaded dual-soliton Stokes, together with the broad pump pulse can cover the entire fingerprint region from 800-1800 cm^{-1}. Fig. 3(b) shows the measured CARS spectrograms of PS beads and PET film. It is worth noting that the powerful combination of spectral focusing and automated delay scanning offers a feasible way to choose vibrational frequency of the molecule of interest. We now can have spectral scanning CARS spectra from 750 to 1150 cm^{-1} for PS when the pump interacts

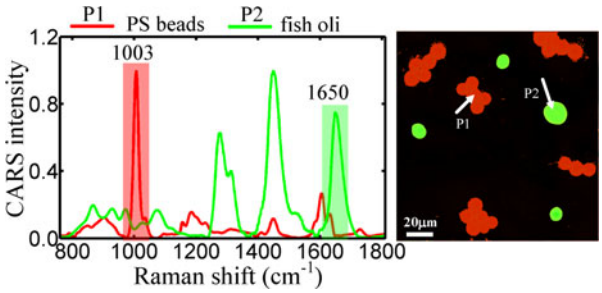

Fig. 4. (a) Normalized CARS spectra obtained for the two different materials pointed out by the arrows. (b) Color coded bead and oil droplets distribution based on the CARS spectral decomposition.

with soliton 1, while it is from 1130 to 1800 cm^{-1} for PET when the pump interacts with soliton 2. We are bringing clear evidences that the two soliton Stokes pulses together with one pump pulse can yield gapless coverage of Raman transitions from 800 to 1800 cm^{-1} while scanning the interpulse delay between the pump and the Stokes beam, as also illustrated in Fig. 2(a). The true CARS spectra are extracted from the three-dimensional spectrograms as the amplitude along the time-delay by integrating the total power of each anti-Stokes spectrum from the spectrometer. Because the pump pulse scans the Stokes soliton 1 and 2 at different time-delay, it enables that spectral CARS information can be encoded and acquired in time without signal aliasing. As shown in Fig. 3(c), CARS signals produced from both soliton 1 and 2 present distorted and typically dissipative spectral lineshape, which is ascribed to the strong NR backgrounds and well-understood in the CARS community. After retrieving the vibrational phase by use of MEM technique, the underlying broad NR background can be subtracted and its output is almost background–free and more resolvable (see Fig. 3(d)). The cascaded dual-soliton Stokes pulses greatly extend CARS spectral coverage and there is considerably more information contained throughout an entire spectrum than at just a single frequency within that spectrum. Thus, we can simultaneously measure the featured Raman resonance of PS and PET at ring breathing (1001 cm^{-1}) and C = C stretch (1665 cm^{-1}). Since the fingerprint vibrational region has profound chemical information, rich chemical information from multiple characteristic vibration in the broad dual-soliton CARS spectrum is more likely to identify molecular structures and helps to explore complicated biochemical processes in cells and tissues.

For spatially inhomogeneous but segregated samples, we show CARS imaging of a mixture of PS beads and fish oil droplets. At every single pixel, a spectrum can be plotted and Fig. 4(a) shows two representative spectra for PS beads or oil droplets (at the arrow point). The phase-retrieved CARS spectra are consistent at different spatial locations and match spontaneous Raman spectra. Besides, CARS spectra of fish oil is also resolved in the crowded Raman region at 1260 and 1300 cm^{-1}. The spectral resolution of CARS can thus be estimated at 15 cm^{-1} from the two Raman peaks. Spectral focusing CARS generally provides a means to optimize the spectral resolution and signal-to-noise ratio [31]. In order to obtain a chemical map of the different kinds of molecules, we use the two CARS spectra as two bases to calculate the concentration of the two species at every pixel location. Fig. 4(b) shows the composite image of beads and droplets based on their calculated concentration, with each color channel corresponding to one species and the intensity corresponding to the concentration. The beads and droplets are well separated with excellent signal-to-noise ratio.

Obviously, the complete spectra scan provides much more detailed information compared to only one piece of Raman shifts from one soliton Stokes pulse. Since the dual-soliton CARS technique measures vibrational signals in both imaging and microspectroscopy, we can perform fast beam-scanning imaging at multiple characteristic vibrational frequencies to obtain more information about the distributions of multiple chemical species. We can also implement microspectroscopy while taking CARS images. We position the laser focus at the point of interest and scan the time delay to obtain these spectra. Thus, we are able to not only acquire chemical images at several important

frequencies in real-time but also perform microspectroscopy at a few positions of interest. Combination of multiple frequency imaging and microspectroscopy will be a powerful tool in the study of complex samples such as cells and tissues, offering more chemical sensitivity and selectivity.

4. Conclusion

In summary, we have presented a new broadband dual-soliton CARS microspectroscopy and microscopy platform with excellent capability of probing the entire fingerprint Raman resonance in one measurement based on a single fiber laser source. Through the use of spectral focusing and in conjunction with automated delay scanning of the pump beam, this system provides a feasible way to choose vibrational frequency of the molecule of interest throughout 800-1800 cm^{-1} region. The combination of the high specificity of broadband CARS with rich information from multiple characteristic vibration peaks allows for excellent identification in hyperspectral imaging of different molecules. Microspectroscopy also greatly helps the image analysis, since multiple chemistry and physical state of different molecules can be simultaneously observed. We believe that this all-fiber-based broadband excitation source may greatly simplify CARS implementation, paving the way towards quantitative label-free chemical imaging integration into widespread biological and material use.

Acknowledgment

The authors would like to thank the anonymous reviewers for their valuable suggestions.

References

[1] E. O. Potma e*t al.*, "Chemical imaging of photoresists with coherent anti-Stokes Raman scattering (CARS) microscopy," *J. Phys. Chem. B* , vol. 108, no. 4, pp. 1296–1301, 2004.
[2] C. H. Camp *et al.*, "High-speed coherent Raman fingerprint imaging of biological tissues," *Nat. Photon.*, vol. 8, no. 8, pp. 627–634, 2014.
[3] M. O. Scully *et al.*, "FAST CARS: Engineering a laser spectroscopic technique for rapid identification of bacterial spores," *Proc. Nat. Acad. Sci. USA*, vol. 99, no. 17, pp. 10994–11001, 2002.
[4] C. L. Evans, E. O. Potma, M. Puoris' haag, D. Côté, C. P. Lin, and X. S. Xie, "Chemical imaging of tissue in vivo with video-rate coherent anti-Stokes Raman scattering microscopy," *Proc. Nat. Acad. Sci. USA*, vol. 102, no. 46, pp. 16807–16812, 2005.
[5] C. L. Evans, E. O. Potma, and X. S. Xie, "Coherent anti-Stokes Raman scattering spectral interferometry: Determination of the real and imaginary components of nonlinear susceptibility χ (3) for vibrational microscopy," *Opt. Lett.*, vol. 29, no. 24, pp. 2923–2925, 2004.
[6] O. Burkacky, A. Zumbusch, C. Brackmann, and A. Enejder, "Dual-pump coherent anti-Stokes-Raman scattering microscopy," *Opt. Lett.*, vol. 31, no. 24, pp. 3656–3658, 2006.
[7] J. Cheng, A. Volkmer, L. D. Book, and X. S. Xie, "Multiplex coherent anti-Stokes Raman scattering microspectroscopy and study of lipid vesicles," *J. Phys. Chem. B*, vol. 106, no. 34, pp. 8493–8498, 2002.
[8] S. Brustlein *et al.*, "Optical parametric oscillator-based light source for coherent Raman scattering microscopy: practical overview," *J. Biomed. Opt.*, vol. 16, no. 2, pp. 021106-1–021106-10, 2011.
[9] F. Ganikhanov, S. Carrasco, X. S. Xie, M. Katz, W. Seitz, and D. Kopf, "Broadly tunable dual-wavelength light source for coherent anti-Stokes Raman scattering microscopy," *Opt. Lett.*, vol. 31, no. 9, pp. 1292–1294, 2006.
[10] J. X. Cheng, Y. K. Jia, G. Zheng, and X. S. Xie, "Laser-scanning coherent anti-Stokes Raman scattering microscopy and applications to cell biology," *Biophys. J.*, vol. 83, no. 1, pp. 502–509, 2002.
[11] C. L. Evans, and X. S. Xie, "Coherent anti-Stokes Raman scattering microscopy: Chemical imaging for biology and medicine," *Annu. Rev. Anal. Chem.*, vol. 1, pp. 883–909, 2008.
[12] K. F. Domke *et al.*, "Host–guest geometry in pores of zeolite ZSM-5 spatially resolved with multiplex CARS spectromicroscopy," *Angew. Chem. Int. Ed.*, vol. 51, no. 6, pp. 1343–1347, 2012.
[13] A. V. Kachynski, A. N. Kuzmin, P. N. Prasad, and I. I. Smalyukh, "Coherent anti-Stokes Raman scattering polarized microscopy of three-dimensional director structures in liquid crystals," *Appl. Phys. Lett.*, vol. 91, no. 15, 2007, Art. no. 151905.
[14] D. Schafer, J. A. Squier, J. van Maarseveen, D. Bonn, M. Bonn, and M. Muller, "In situ quantitative measurement of concentration profiles in a microreactor with submicron resolution using multiplex CARS microscopy," *J. Amer. Chem. Soc.*, vol. 130, no. 35, pp. 11592–11593, 2008.
[15] M. Windbergs, M. Jurna, H. L. Offerhaus, J. L. Herek, P. Kleinebudde, and C. J. Strachan, "Chemical imaging of oral solid dosage forms and changes upon dissolution using coherent anti-Stokes Raman scattering microscopy," *Anal. Chem.*, vol. 81, no. 6, pp. 2085–2091, 2009.

[16] C. W. Freudiger, W. Yang, G. R. Holtom, N. Peyghambarian, X. S. Xie, and K. Q. Kieu, "Stimulated Raman scattering microscopy with a robust fibre laser source," *Nat. Photon.*, vol. 8, no. 2, pp. 153–159, 2014.
[17] E. Andresen, P. L. Berto, and H. Rigneault, "Stimulated Raman scattering microscopy by spectral focusing and fiber-generated soliton as Stokes pulse," *Opt. Lett.*, vol. 36, no. 13, pp. 2387–2389, 2011.
[18] E. Andresen, V. Birkedal, J. Thøgersen, and S. R. Keiding, "Tunable light source for coherent anti-Stokes Raman scattering microspectroscopy based on the soliton self-frequency shift," *Opt. Lett.*, vol. 31, no. 9, pp. 1328–1330, 2006.
[19] S. Saint-Jalm, P. Berto, L. Jullien, E. Andresen, and H. Rigneault, "Rapidly tunable and compact coherent Raman scattering light source for molecular spectroscopy," *J. Raman Spectrosc.*, vol. 45, no. 7, pp. 515–520, 2014.
[20] P. Adany, D. C. Arnett, C. K. Johnson, and R. Hui, "Tunable excitation source for coherent Raman spectroscopy based on a single fiber laser," *Appl. Phys. Lett.*, vol. 99, no. 18, 2011, Art. no. 181112.
[21] E. Andresen and H. Rigneault, "Soliton dynamics in photonic-crystal fibers for coherent Raman microspectroscopy and microscopy," *Opt. Fiber Technol.*, vol. 18, no. 5, pp. 379–387, Sep. 2006.
[22] J. Su, R. Xie, C. K. Johnson, and R. Hui, "Single-fiber-laser-based wavelength tunable excitation for coherent Raman spectroscopy," *J. Opt. Soc. Amer. B*, vol. 30, no. 6, pp. 1671–1682, 2013.
[23] M. Lehtonen, G. Genty, and H. Ludvigsen, "Supercontinuum generation in a highly birefringent microstructured fiber," *Appl. Phys. Lett.*, vol. 82, no. 14, pp. 2197–2199, 2003.
[24] K. Chen, T. Wu, H. Wei, and Y. Li, "Dual-soliton Stokes-based background-free coherent anti-Stokes Raman scattering spectroscopy and microscopy," *Opt. Lett.*, vol. 41, no. 11, pp. 2628–2631, 2016.
[25] F. R. Arteaga-Sierra, C. Milian, I. Torres-Gomez, M. Torres-Cisneros, G. Molto, and A. Ferrando, "Supercontinuum optimization for dual-soliton based light sources using genetic algorithms in a grid platform," *Opt. Exp.*, vol. 22, no. 19, pp. 23686–23693, 2014.
[26] G. P. Agrawal, *Nonlinear Fiber Optics*, 5th ed. Oxford, U.K.: Academic, 2013.
[27] K. Chen, T. Wu, H. Wei, T. Zhou, and Y. Li, "Dual-soliton Stokes-based background-free coherent anti-Stokes Raman scattering spectroscopy and microscopy," *Biomed. Opt. Exp.*, vol. 7, no. 10, pp. 3927–3939, 2016.
[28] L. Brückner, T. Buckup, and M. Motzkus, "Exploring the potential of tailored spectral focusing," *J. Opt. Soc. Amer. B*, vol. 33, no. 7, pp. 1482–1491, 2016.
[29] T. Hellerer, A. M. K. Enejder, and A. Zumbusch, "Spectral focusing: High spectral resolution spectroscopy with broad-bandwidth laser pulses," *Appl. Phys. Lett.*, vol. 85, no. 1, pp. 25–27, Feb. 2004.
[30] I. Rocha-Mendoza, W. Langbein, P. Watson, and P. Borri, "Differential coherent anti-Stokes Raman scattering microscopy with linearly chirped femtosecond laser pulses," *Opt. Lett.*, vol. 34, no. 15, pp. 2258–2260, Sep. 2009.
[31] A. F. Pegoraro, A. Ridsdale, D. J. Moffatt, Y. Jia, J. P. Pezacki, and A. Stolow, "Optimally chirped multimodal CARS microscopy based on a single Ti: Sapphire oscillator," *Opt. Exp.*, vol. 17, no. 4, pp. 2984–2996, Apr. 2009.
[32] L. Brückner, T. Buckup, and M. Motzkus, "Enhancement of coherent anti-Stokes Raman signal via tailored probing in spectral focusing," *Opt. Lett.*, vol. 40, no. 12, pp. 5204–5207, Sep. 2015.
[33] H. A. Rinia, M. Bonn, M. Müller, and E. M. Vartiainen, "Quantitative CARS spectroscopy using the maximum entropy method: The main lipid phase transition," *Chem. Phys. Chem.*, vol. 8, no. 2, pp. 279–287, Feb. 2007.